



## Improved active anticorrosion coatings using layer-by-layer assembled ZnO nanocontainers with benzotriazole

S.H. Sonawane<sup>c,\*</sup>, B.A. Bhanvase<sup>a</sup>, A.A. Jamali<sup>a</sup>, S.K. Dubey<sup>a</sup>, S.S. Kale<sup>a</sup>, D.V. Pinjari<sup>b</sup>, R.D. Kulkarni<sup>c</sup>, P.R. Gogate<sup>b</sup>, A.B. Pandit<sup>b</sup>

<sup>a</sup> Vishwakarma Institute of Technology, 666, Upper Indira Nagar, Pune 411 037, India

<sup>b</sup> Institute of Chemical Technology, N. P. Marg, Matunga, Mumbai 400019, India

<sup>c</sup> Chemical Technology Department North Maharashtra University Jalgaon, 425001 India

### ARTICLE INFO

#### Article history:

Received 5 October 2011

Received in revised form 8 February 2012

Accepted 25 February 2012

#### Keywords:

Nanocontainers

ZnO Core, L-b-L assembly

Corrosion inhibitor, Release rate

### ABSTRACT

In the present work, a novel approach for the synthesis of nanocontainers by encapsulation has been presented, which are capable of responsive release of corrosion inhibitors (benzotriazole). Nanocontainers have been prepared using layer-by-layer (LbL) assembly of oppositely charged species of polyelectrolytes and inhibitor on the surface of ZnO. Synthesis of nanostructured zinc oxide was carried out initially using the sonochemical precipitation approach. The thickness of the layer, surface charge and functional groups present on each layer were identified using particle size distribution (PSD), zeta potential and FTIR analysis, respectively. The average initial size of the core ZnO was in nanosize range as observed in the TEM image. XRD analysis shows that ZnO contains wurtzite as a major phase. The release properties of polyelectrolyte modified ZnO nanocontainer have been investigated and the observed release rate characteristics show that these nanocontainers would be useful in the multifunctional coating formulations. Responsive release of inhibitor was quantitatively evaluated in water at different pH. Performance of nanocontainers was studied in corrosive environment by incorporating the nanocontainers in alkyd resin. Results of UV-spectroscopy at different pH, corrosion rate analysis and TAFEL plots of nanocontainers coatings on mild steel (MS) panel have been presented. It has been found that electrochemical current density decreased from 0.00355 to 0.0008 A/cm<sup>2</sup>, when neat alkyd resin combined with 5% nanocontainers has been used in the coating. Corrosion results from Tafel plot and corrosion rate analysis shows that the 5 wt% loading of nanocontainers is useful and optimum for the sustained release of inhibitor for the applications in the marine coatings irrespective of the operating pH.

© 2012 Elsevier B.V. All rights reserved.

## 1. Introduction

Corrosion is one of important technological problem faced by all the industries such as manufacturing, chemical and petrochemical industries. Three possible approaches are being used to protect the metal surfaces from corrosion i.e. by cathodic protection, anodic protection (passivation technique) and barrier mechanism [1,2]. Dense barrier coatings show low permeability to the corrosive chemicals and hence barrier coatings are generally used for corrosion protection [3]. Corrosion inhibitor additives can be easily incorporated into paint formulation, which can generate additional protective layer on the surface. In the case of active corrosion pro-

tection (ACP) system, anticorrosion agents especially liquids are being introduced into the coatings [4]. However, direct addition of these liquid inhibitors affects the performance of these doped coatings [5].

Encapsulation of active materials loaded on core or in the hollow lumen of microcapsule/nanocontainer is one of the important concepts, which offers additional advantage of selective release of the active ingredients on demand [6–13]. These polyelectrolyte containers are being used in number of applications such as biomedical [14], drug delivery [15], catalyst [16], textile, etc. to deliver ingredients in a sustained manner. Encapsulation process and preparation of nanocontainers and its application in corrosion inhibition has been investigated by number of researchers [7,8,10–13,17–22]. The most important advantage of the use of nano/micro reservoir systems lies in responsive and sustainable release of inhibitor. Some of the liquid inhibitors, which cannot be used directly in the coatings formulation as these inhibitors react with the coating, can be effectively stored in micro or nano-container using encapsulation.

\* Corresponding author. Tel.: +91 20 25601271.

E-mail addresses: [shirishsonawane@rediffmail.com](mailto:shirishsonawane@rediffmail.com) (S.H. Sonawane), [dr.pandit@gmail.com](mailto:dr.pandit@gmail.com) (A.B. Pandit).

<sup>1</sup> Currently working in Department of Technology University of Pune.

Different trigger mechanism can be initiated for the responsive release of these inhibitors which may depend on pH, temperature, mechanical stimulation or their combinations. The use of nanocontainer has some disadvantages such as (1) containers should be dispersible with coating vehicle and remain intact on capsules, (2) containers should be compatible with coating formulation, (3) loading of containers should not affect the other application properties of coatings, (4) release kinetics should be fast in case of healing mechanism, while it should be sustainable in the case of responsive release and (5) added container quantity should be minimal so that it should not affect pigment volume concentration (PVC ratio).

There are number of ways of introducing containers for anti-corrosion activity. Layer by layer (LbL) assembly of polyelectrolyte has been reported by Shchukins et al. [20]. In LbL approach, films containing one or several polyelectrolyte monolayers can be assembled on the surface of a template (e.g., polyelectrolyte capsules), which possess controlled permeability properties. A nano structured multifunctional shell can be prepared using LbL assembly of oppositely charged species (polyelectrolytes and nanoparticles) on the surface of the precursor. These smart nanocontainers release the inhibitor on demand. In the work of Shchukin et al. [20], inorganic halloysite of diameter of 25 nm has been used to encapsulate the inhibitor. These tubes are having a layer of positive and negative charges on outside and inside surface (at pH 8) of lumen respectively, which helps in protecting the inhibitor and releasing the same to outside environment when required. Shchukin et al. [22] used halloysite nanotubes with inner voids loaded with inhibitor. The outer surface was covered with layer-by-layer polyelectrolyte multilayer using hybrid sol-gel synthesis. Core and shell morphology using emulsion method has also been reported [22,23]. LBL halloysite nanocontainer is probably the best approach to use for long term and sustained release applications [22]. Inorganic core based nano containers could be spherical in shape with a typical diameter in the range of 50–200  $\mu\text{m}$ . In the case of layer by layer assembly of inorganic core, functionalized silica/polymer may be used and inhibitor is loaded in the layered assembly of polyelectrolytes [4,11,20,23]. Shchukin et al. [20,23] formulated a benzotriazole-loaded polyelectrolyte capsule. Layers of Polyelectrolytes were formed on the surface of the negatively charged  $\text{SiO}_2$  nanoparticles. Ultrasound assisted electrochemical method has been used to synthesize hollow sphere of conducting polymer such as polypyrrole in which inhibitor can be loaded [19]. Abu and Aoki [24] and Shchukin et al. [25] have used electrochemical deposition method for the preparation polyaniline-coated polystyrene latex of 1.85  $\mu\text{m}$  size. These latex particles were used for the corrosion protection of the iron plate in 3%, w/v NaCl aqueous solution. Cavitation bubble as a template was used for the fabrication of nanocontainers, on which an organic or inorganic shell is formed from precursors, during the sonication of the reaction mixture [23]. Tomalino and Bianchini [26] have prepared container-based active coatings, which were directly fabricated on a metal surface of heat-expandable spheres for car metallic protection based on ethyl vinyl acetate derivatives, diatomaceous earth and zeolite, and hollow silica microparticles.

The use of the conductive polymers as building blocks for micro and nanocontainers with the shell sensitive to the electrochemical potential has also been reported [27]. In the case of self healing coating, when there is scratch or a crack on the coatings, inhibitor release takes place based on the response to change in pH or intensity of light. This serves to protect the metal structure at the defect site by self healing mechanism or by neutralizing the ions [6,8,12,13,17–20,28–30]. In earlier reports, Borisova et al. [4] described mesoporous silica as an inorganic core, but in fact anti-corrosive properties introduced by silica is not similar to corrosion inhibitor pigment property as introduced by ZnO. Zinc oxide is

expected to form a passive layer in contact with water and oxygen, which can inhibit the flow of electrons from anode to cathode [31,32] and hence the metal surface is protected. The other oxides such as antimony oxide, titanium dioxide, iron oxide etc. do not form such passive layer as efficiently as ZnO. There have been some earlier reports depicting the use of semiconductor oxide particles such as ZnO in the coatings to enhance anticorrosion performance through passivation mechanism [31]. Zinc oxide has been confirmed to exhibit anticorrosion capacity by accepting electrons from the metal [32]. Also ZnO offers other advantages such as low cost and environmental friendly nature as compared to the chromate based pigments. With this background, ZnO has been selected as an inorganic core to prevent the corrosion reactions at the metal-coating interface, whereas polyaniline and PAA have been used in the container assembly so that even if the formed coatings are removed these anticorrosive materials still remain effective.

The approach based on the use of ZnO for nanocontainer has not been reported in the literature. In order to take the dual advantage of the anticorrosive pigment and inhibitor loaded onto a single shell, ZnO was used as a core of the container, which works as an anodic-type inhibitor as well as a good nano-filler, which significantly inhibits the corrosion of the bare steel as an anodic protector. Further, in case the electrolyte shell containing inhibitor becomes inactive, ZnO core will still remain active against the corrosive species. An attempt has been made to demonstrate the possibility to employ ZnO particles coated with polyaniline/benzotriazole/polyacrylic acid layers as a prospective nanocontainer embedded in alkyd resin coating. The inhibitor (benzotriazole) is entrapped between the two polyelectrolytes (polyaniline and PAA) layers. In the present work, polyaniline (PANI) has been used as a polyelectrolyte. It has been reported that PANI also has inhibiting effect due to the formation of a compact iron/dopant complex layer at the metal-coating interface, which acts as a passive protective layer having a redox capability to undergo a continuous charge transfer reaction at the metal-coating interface, in which PANI is reduced from emeraldine salt form (ES) to an emeraldine base (EB) [33]. The resulting hybrid film has a pronounced protective efficiency for the corrosion inhibition. The release properties of inhibitor have been investigated using UV spectroscopy in aqueous media at different pH for the low molecular weight benzotriazole. Uniform release and long term active corrosion protection of MS has been confirmed with the actual example of benzotriazole loaded ZnO nanocontainers dispersed into alkyd resin.

## 2. Experimental

### 2.1. Materials

Analytical grade chemicals such as zinc nitrate ( $\text{Zn}(\text{NO}_3)_2$ ), sodium hydroxide, benzotriazole, HCl, NaOH, NaCl and ethanol have been procured from Sigma Aldrich and used as received from the supplier. Polyacrylic acid (PAA,  $M_w = 50\,000\text{ g mol}^{-1}$ ) was also procured from Sigma-Aldrich. The monomer aniline (analytical grade, M/s Fluka) was distilled two times prior to use. Ammonium persulphate (APS,  $(\text{NH}_4)_2\text{S}_2\text{O}_8$ ) as a polymerization initiator and surfactant, Sodium Dodecyl Sulfate (SDS,  $\text{NaC}_{12}\text{H}_{25}\text{SO}_4$ ) were procured from S. D. Fine Chem., Mumbai and were used without further purification. Long Oil Soy Alkyd resin (Industrial grade) was procured from M/s Mahuli Paints, Pune, India. Demineralized water prepared using Millipore apparatus was used during all the experimental runs.

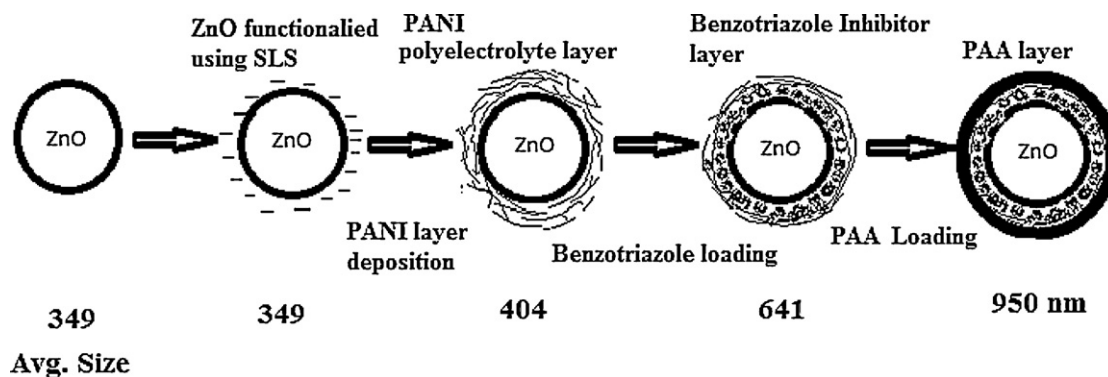


Fig. 1. Schematic illustration of the procedure for benzotriazole loading on ZnO nanoparticulate containers.

## 2.2. Preparation of ZnO nanocontainers

Sonochemical synthesis of zinc oxide nanoparticles has been performed initially as per the detailed procedure described in our earlier work [30]. Using these nanoparticles, ZnO nanocontainers have been synthesized using a multi-step approach as outlined below:

- (1) Formation of polyaniline (PANI) layer on ZnO core using in situ emulsion polymerization: in the layer-by-layer assembly of ZnO nanocontainer, ZnO was used as a core based on the anticorrosion properties. Initially ZnO nanoparticles have been functionalized using SDS surfactant so that a negative charge is obtained on the surface of ZnO. Ultrasound assisted in situ miniemulsion polymerization has been then used for the deposition of PANI layer on the ZnO core [31,32] with an objective of obtaining complete coverage of ZnO surface by PANI. Initially, surfactant solution was prepared with an addition of 0.3 g sodium dodecyl sulfate (SDS) and 0.5 g ZnO nanoparticles in 50 mL of water and taken in a reactor. The initiator solution was prepared separately by adding 0.7 g ammonium persulphate (APS) in 10 mL of deionized water and transferred to the same reactor. In order to eliminate the inhibition effect of oxygen on polymerization reaction, reaction mixture was purged with argon gas initially for 20 minutes. Further, dropwise addition of a total quantum of aniline as 5 g was achieved over a period of 30 min. After this addition, the reaction mixture was subjected to ultrasonic irradiations (Hielscher Ultrasonics GmbH, 22 kHz frequency and 240 W rated power) in the reactor, which was maintained at a temperature of 4 °C throughout the reaction time of 60 min. Resulting PANI coated ZnO nanoparticles were separated by centrifugation at 4000 rpm for a period of 30 min and washed with water followed by acetone. Synthesized PANI coated ZnO materials was incubated in 0.5 M NaCl solution doped with 1 wt% polyvinyl pyrrolidone (PVP) in ethanol for 20 min to prevent aggregation of the formed particles. Resulting PANI coated ZnO particles were washed with water and separated by centrifugation after the incubation step.
- (2) Loading of benzotriazole (anticorrosion agent) on PANI coated ZnO: prepared PANI coated ZnO material was added into 0.1 N NaCl solution prepared in 100 mL water. The loading of benzotriazole shell (third layer) on PANI-ZnO particles was achieved using 10 mg mL<sup>-1</sup> of benzotriazole in the acidic media (pH = 3) for 20 min. Benzotriazole loaded PANI-ZnO nanoparticles were separated by centrifugation.
- (3) Deposition of polyelectrolyte layer (Polyacrylic acid) on benzotriazole loaded PANI-ZnO nanoparticles: in order to increase the compatibility of the nanocontainers in resin, the final polyacrylic acid polyelectrolyte layer was added after the loading of

benzotriazole on PANI layer. The adsorption of the negatively charged polyacrylic acid was achieved on benzotriazole loaded PANI-ZnO nanoparticles using 2 mg mL<sup>-1</sup> polyacrylic acid solution in 0.5 M NaCl for a period of 20 min. Finally, the resulting nanocontainer was separated by centrifugation and then dried in an oven at 60 °C for 48 h.

Thus, the layer-by-layer assembly of polyelectrolyte was prepared and benzotriazole inhibitor was loaded in between the layers of PANI and polyacrylic acid, whereas ZnO nanoparticles were used as the core of the assembly. The formation mechanism of ZnO nanocontainer has been reported in Fig. 1.

## 2.3. Preparation of nanocontainer/alkyd coatings

Nanocontainer-alkyd coatings were prepared using pigment muller and by dispersing 2.0, to 5.0 wt% of the synthesized nanocontainers in the alkyd resin. The prepared coating was thoroughly mixed with acetone solution to ease the procedure of application of coating by using bar coater on MS panels having dimensions 70 mm × 50 mm × 1 mm.

## 2.4. Characterization of nanocontainer and nanocontainer/alkyd coatings

XRD diffraction patterns of ZnO and Nanocontainer were recorded by using powder X-ray diffractometer (Philips PW 1800). Transmission electron microscopy (TEM) of nanocontainer was performed on Technai G20 working at 200 kV. Release of corrosion inhibitor benzotriazole at different pH was measured using UV-vis spectrophotometer (SHIMADZU 160A model). A UV spectrophotometer has been used to determine the concentration of benzotriazole in water. Initially the calibration curve was plotted for different concentrations over the range 0.01 to 1 mg/L of benzotriazole. 0.2 g of nanocontainer per 20 mL of water was added into the water for different pH conditions. The benzotriazole concentration was measured in water using the absorbance value. The concentration of benzotriazole has been reported in mg of benzotriazole released per g of nanocontainer added per litre of water.

FTIR analysis of samples were carried out (SHIMADZU 8400S) in the region of 4000–500 cm<sup>-1</sup>. The particle size distribution and electrophoretic mobility measurements were carried out by Malvern Zetasizer Instrument (Malvern Instruments, Malvern, UK). The thickness of the coating film on MS plate was maintained close to 50 μm. Corrosion tests were conducted in acid, alkali, and salt solution (HCl, NaOH, NaCl: 5 wt% each) by placing the MS strips in porcelain dishes and coated samples were immersed in test media till observable deterioration occurred. Each sample was under media for nearly 200 h. The protective behavior of corrosion

inhibitor against the dissolution of MS was evaluated by calculating the corrosion rate ( $V_c$ ) in cm/year for each sample [34] using the expression

$$V_c = \frac{\Delta g}{Atd} \quad (1)$$

where  $\Delta g$  is the weight loss in gram for each sample,  $A$  is the exposed area of the sample in  $\text{cm}^2$ ,  $t$  is the time of exposure in years, and  $d$  is the density of the metallic species in  $\text{g/cm}^3$ . The weight loss was measured after carefully washing the samples with water till the deposited corrosion products were removed, and finally, moisture was removed from the samples by drying the same at  $60^\circ\text{C}$  ( $\pm 1$ ) in an oven till constant weight.

All electrochemical measurements have been performed on computerized electrochemical analyzer (supplied by Autolab Instruments, Netherlands). An MS panel was used as the working electrode with a platinum sheet as the counter and a saturated calomel electrode (SCE) as the reference electrode. The MS panel was cleaned initially and five different MS plates were coated with neat alkyd resin. 2–5% of nanocontainer dispersed in the same alkyd resin was used as working electrode and about  $1\text{ cm}^2$  of area was used for sample testing of the working electrode. Polarization measurements were taken after exposure to the 0.5 M NaCl solution. The potential was scanned between  $-2\text{ V}$  to  $+2\text{ V}$  at a rate of  $2\text{ mV/s}$ . Electrochemical measurements were carried out at room temperature ( $25^\circ\text{C}$ ).

### 3. Results and discussions

Fig. 2a shows the Zeta ( $\zeta$ ) potential of each layer of the LbL assembly in water. Initially ZnO nanoparticles were coated with the SDS. Electrophoretic measurements indicate that initially on the ZnO particles, charges were near to the value of  $\approx -3.37\text{ mV}$ . Further addition of the PANI layer shows the slight increase in the negative value of Zeta potential ( $\approx -3.73\text{ mV}$ ). Though PANI introduces positive charges on the surface, due to the presence of SDS during polymerization, additional layers do not show an increase in the value of zeta potential. During miniemulsion polymerization, monomer aniline enters the micelle and occupies the space near to the head group of the adsorbed SDS rather than the hydrophobic tail region [35]. This phenomena leads to a reduction in the head group packing for SDS, which also leads to a reduction in SDS adsorption resulting into reduction in the layer thickness and zeta potential. The phenyl moiety resides within the hydrophobic region and the polar group remains between the SDS head groups as also recently reported by Kim et al. [36]. Further, Salgaonkar and Jayaram [37] have also reported the formation of polyaniline film in the presence of HCTAB surfactant. It has been reported that the surfactant adsorption strongly depends on the concentration of aniline and an increase in the aniline concentration results in a decrease in the amount of surfactant adsorption on  $\text{ZrO}_2$  which in turn does not show any change in the zeta potential value [37]. Further, addition of benzotriazole show a drastic increase in zeta potential value which is near to  $\approx -22\text{ mV}$ . Addition of polyacrylic acid decreases the zeta potential value near to  $\approx -12.8\text{ mV}$ .

The value of zeta potential is a strong indication of the adsorption of charged species and intra-particle interaction. In the present work, the possibility of incomplete charging of the surface by PANI has been avoided by the addition of benzotriazole, which is also confirmed by the fact that there is an increase in the zeta potential after the addition of benzotriazole [38]. The increase in the value of zeta potential and hence enhanced charging of the surface of layer by liquid benzotriazole indicates the deep penetration of benzotriazole into the PANI layer. As shown in Fig. 2b, nanocontainer show that the average particle size gradually increases. This clearly indicates and confirms the layer by layer building of the

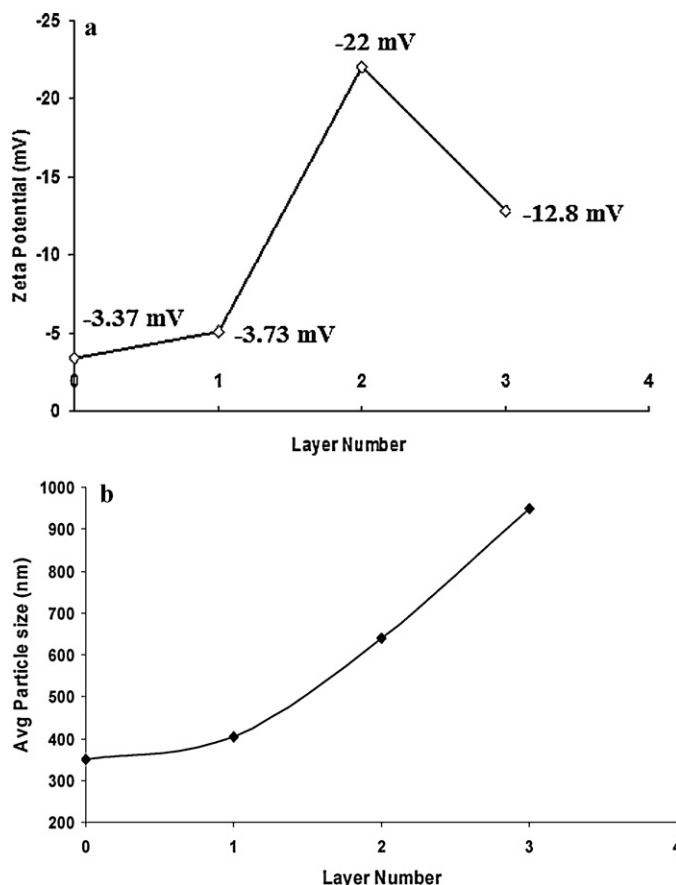


Fig. 2. (a) Electrophoretic mobility measurements of nanocontainer in water during LbL assembly. Layer number 0: initial ZnO, 1: ZnO/PANI, 2: ZnO/PANI/Benzotriazole, 3: ZnO/PANI/Benzotriazole/PAA. (b) Growth in particle size of nanocontainer during LbL assembly. Layer number 0: initial ZnO, 1: ZnO/PANI, 2: ZnO/PANI/Benzotriazole, 3: ZnO/PANI/Benzotriazole/PAA.

nanocontainer by following the procedure described in Section 2.2. Malvern particle size analyzer has been used for these measurements. Initially, the particle size of the ZnO nanoparticle support was found to be around  $349\text{ nm}$ . After the formation of PANI layer onto ZnO nanoparticles by the miniemulsion polymerization, it has been observed that the particle size increased to an average value of  $404\text{ nm}$ . Therefore, it can be said that the thickness of layer of PANI show an average thickness of  $28\text{ nm}$  (as per analysis taken from dynamic light scattering method). Addition of the benzotriazole molecular layer increases the thickness further by  $119\text{ nm}$ . Benzotriazole layer thickness is high, which clearly indicates that a large number of molecules were adsorbed on PANI coated ZnO particles assembly as the benzotriazole is a small molecule than the PANI layer. Finally the chains of the PAA were embedded onto the benzotriazole layers with an average thickness of  $150\text{ nm}$  size. Increase in the size with an increase in layer thickness indicates the complete formation of the nanocontainer assembly as schematically shown in Fig. 1. The average size of the nanocontainer was found to be about  $950\text{ nm}$  as indicated by PSD analysis. The surface characterization of the nanocontainer has been depicted in Fig. 3 in the form of TEM images. The dark black spots in the image (Fig. 3) indicate the presence of ZnO at the core and it is surrounded by the layers of polyelectrolyte and corrosion inhibitor (benzotriazole). It has also been confirmed that due to the presence of electrolyte and the change in surface charge and energy, multiple particles agglomerate to make a bigger particle with average size of about  $900\text{ nm}$ . The change in the intensity of light around each particle shows that PANI/benzotriazole/PAA layers were separately deposited on the

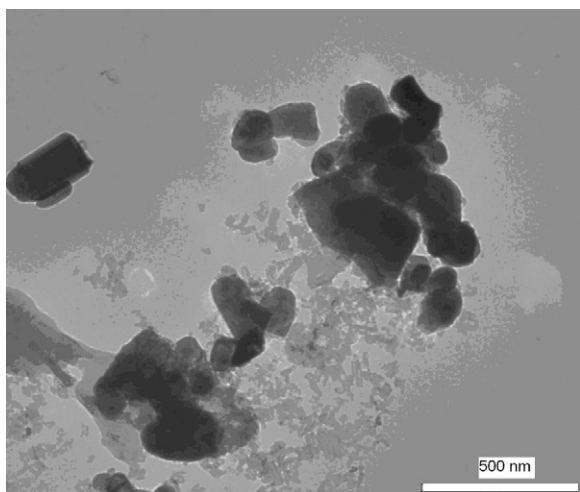


Fig. 3. TEM Image of ZnO nanocontainer showing average size of container near to 900 nm.

ZnO nanoparticles. Preparation of layer by layer assembly of ZnO nanocontainer and covering of organic layer on ZnO nanoparticle has been confirmed from the PSD analysis and growth of particle as represented in Fig. 2b. Increment in the size of particles with the number of deposited layers confirms the presence of organic molecules around the ZnO core. Shchukin and Mohwald [23] have reported a similar approach of analysis in terms of the coverage by organic molecules and growth of particle size.

Fig. 4 depicts the FTIR spectrum of ZnO loaded with PANI (pattern A), ZnO loaded with PANI and Benzotriazole (pattern B) and ZnO loaded with PANI-Benzotriazole-Polyacrylic acid (pattern C). Fig. 4 shows a layer of SDS formed on ZnO nanoparticles initially, which is shown by the peaks at 2646, 1896, 1743, 1298.4 and 1093.67  $\text{cm}^{-1}$ . Fig. 4 (pattern A) confirms the formation of Polyaniline on the ZnO nanoparticles. The peaks at 3506, 3408 and 3342  $\text{cm}^{-1}$  are the characteristic peaks of polyaniline, indicating that polyaniline has been formed on the surface of ZnO nanoparticles. The peaks at 3506.7 and 2995  $\text{cm}^{-1}$  are due to the  $\text{NH}_2$  stretching and C–H bonds, respectively. The spectra in Fig. 4 (pattern B), is the one after loading of benzotriazole. The peaks at 1400, 1278, 1203, 1120.68 and 768  $\text{cm}^{-1}$  show the benzotriazole layer formation. The bands close to 786  $\text{cm}^{-1}$  are typical of the benzene ring vibrations and the band near to 1400  $\text{cm}^{-1}$  is characteristic of the aromatic and the triazole ring stretching vibrations [39]. In

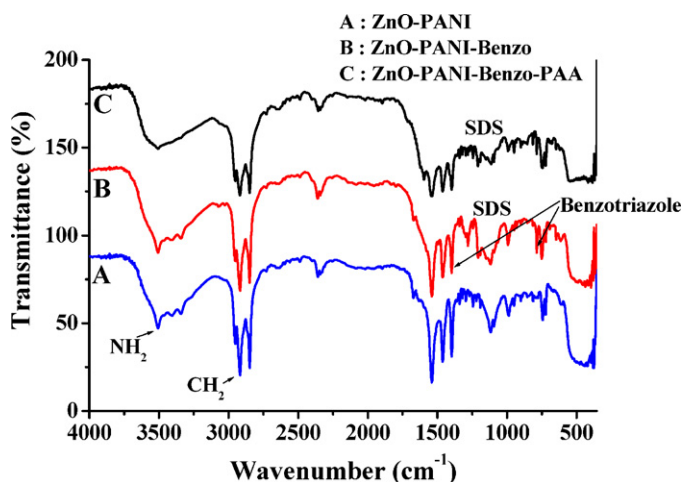


Fig. 4. FTIR spectra of: (a) ZnO loaded with PANI, (b) ZnO loaded with PANI and benzotriazole, (c) ZnO loaded with PANI, benzotriazole and PAA (Polyacrylic acid).

Fig. 4 (pattern C), it is observed that the peaks of the PANI (3408 and 3342  $\text{cm}^{-1}$ ), as seen in Fig. 4 (pattern B), are not observed as benzotriazole and PAA interfered with PANI chains.

Fig. 5A depicts the XRD pattern of ZnO and ZnO loaded with polyelectrolytes and Benzotriazole. The formation of ZnO encapsulated nanocontainers has been depicted in the figure and it can be also observed that during the preparation of nanocontainers, ZnO phase remains the same. The XRD pattern of the ZnO (pattern a) and ZnO loaded with PANI-Benzotriazole-Polyacrylic acid (pattern b) shows that ZnO nano particles is wurtzite, hexagonal in structure. It is also indicated by well indexed XRD peaks corresponding to the planes (101), (100), (002) and no other peaks of impurities were observed [40]. Furthermore the diffraction peaks were more intense and narrower, implying a good crystalline nature of ZnO powder. The crystallite size for ZnO calculated by using Scherrer's formula comes out to be 41.29 nm and for ZnO loaded with polyelectrolytes and inhibitor the size is 45.56 nm.

Fig. 5(B) demonstrates the DTA diagram of zinc oxide and zinc oxide nanocontainers. Two endothermic peaks at 57 °C and 137 °C of the ZnO nanoparticles are attributed to the removal of physically adsorbed water. In the range from 50 to 130 °C, the water molecules interacting with ZnO surface in the form of hydroxyl group interaction are released from the ZnO structure [41]. The exothermic peak at 423 °C is due to the presence of zinc nitrate and sodium hydroxide in small quantity used to form ZnO. DTA of ZnO nanocontainers shows small endothermic peaks at 135 °C, which is attributed to the removal of water. Exothermic peaks at 300–450 °C shows multistage decomposition of PAA, PANI and Benzotriazole (inhibitor), which is supported by thermogravimetric analysis (Fig. 5C). A sharp peak in the range between 300 to 450 °C corresponds to oxidative degradation of PAA, PANI and benzotriazole [42] as reported in Fig. 5C. Fig. 5C shows the decomposition of the ZnO nanocontainer as indicated by a weight loss in the range of 35–450 °C. ZnO and its nanocontainer show the difference in the decomposition above 150 °C, the hydroxyl molecules are being removed in case of ZnO while electrolyte layers starts decomposing in the case of nanocontainer. 70% of the materials show thermal stability above 350 °C temperature.

### 3.1. Release study of inhibitor from nanocontainer into aqueous media

Benzotriazole acts as inhibitor for ferrous metals under acidic conditions [43–45] as well as under neutral conditions [46,47]. In acid solutions the inhibition of iron results from the adsorption of benzotriazole in its molecular or protonated form with the formation of compact passive layer [45,46]. Benzotriazole gives better corrosion inhibition in acidic medium; therefore release performance of the benzotriazole containing nanocontainers were studied in aqueous media of 3, 5, 7 pH which was adjusted using acidic buffer solutions. Objective of the investigation is to find out the optimum pH conditions at which the release reaches to a maxima and to validate that these nanocontainers shows the responsive release. Percent release of the corrosion inhibitor at different pH was measured using UV–vis spectrophotometry analysis. The release study was performed for about 8 h. As shown in Fig. 6, at any operating pH, a stable release is observed after 7 h (all pH values), which indicates that the prepared nanocontainer shows proper encapsulation of the benzotriazole into the polyelectrolyte (PANI) layer. Maximum release at 8 h (0.86  $\text{mg L}^{-1} \text{g}^{-1}$  of ZnO nanocontainer) was found in the case of operating pH as 3, while only a minimal release (0.10  $\text{mg L}^{-1} \text{g}^{-1}$  of ZnO nanocontainer) was observed at 11 pH (not shown) after 8 h. At neutral pH, the release was 0.36  $\text{mg L}^{-1} \text{g}^{-1}$  of ZnO nanocontainer, which is intermediate between the acidic and alkaline conditions.

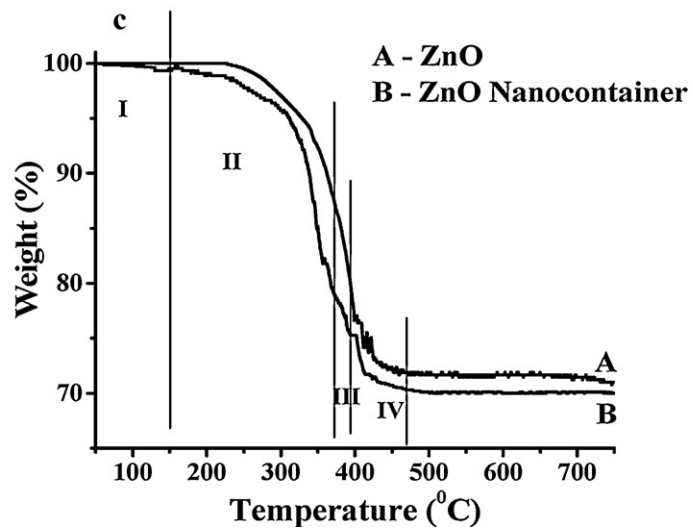
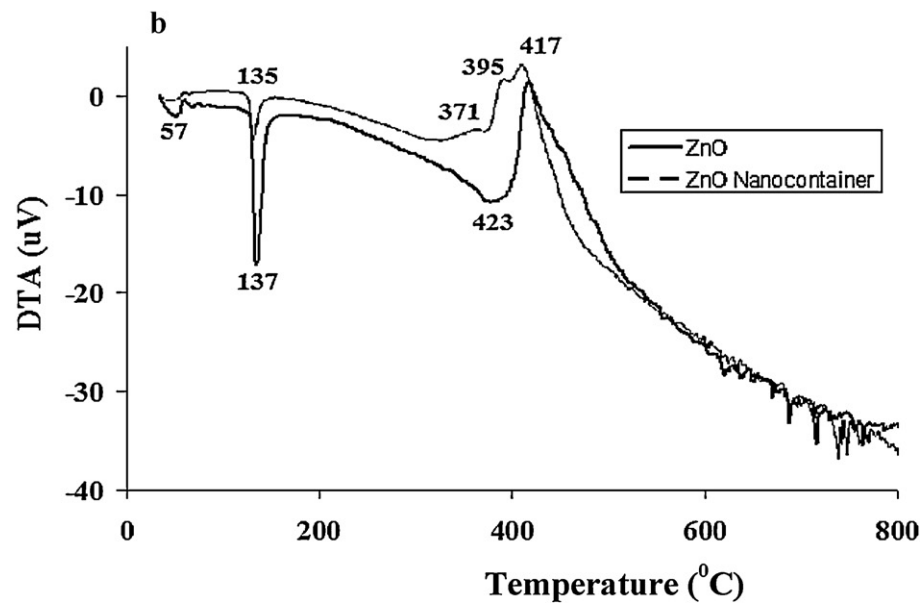
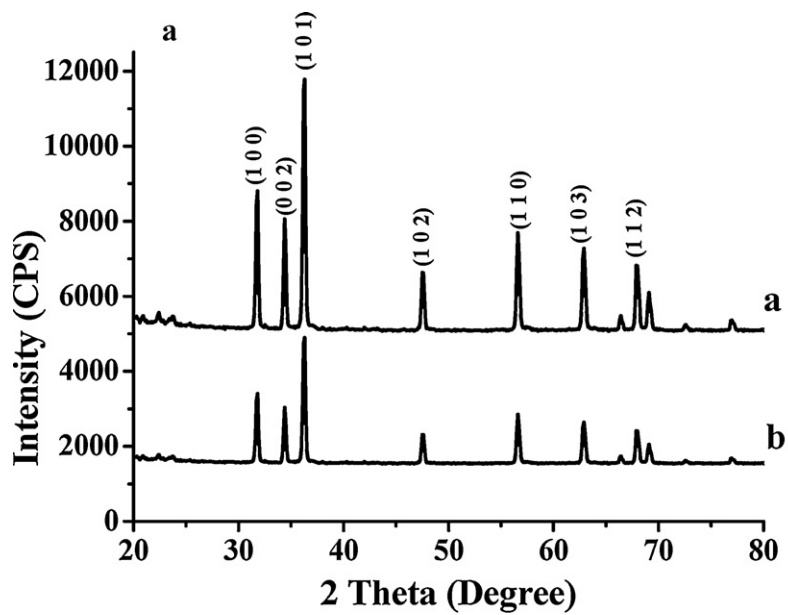


Fig. 5. Comparison of neat ZnO particles and ZnO nanocontainers using XRD (A), DTA analysis (B) and TGA analysis (C).

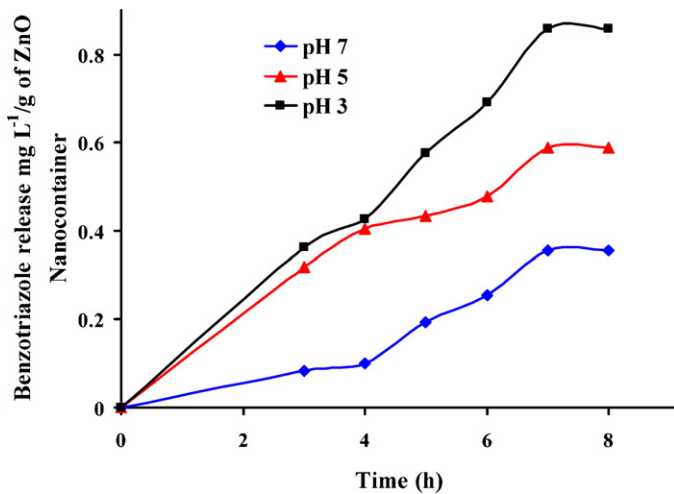


Fig. 6. Release of benzotriazole from nanocontainers at three different pH values.

### 3.2. Corrosion rate analysis of nanocontainer containing coatings

Corrosive environment accelerates under reduced pH (acidic conditions) or increased pH (alkaline conditions). Acid or alkali may attack the binder causing its degradation by hydrolysis or other chemical reactions. The degradation of polymer may facilitate the penetration of oxygen and moisture through the film and reduction of adhesion of coating to the substrate. It is well known that the strong corrosion resistance requires strong adhesion character and hence the weight loss method is an indirect method of evaluation of corrosion resistance under actual conditions of application. There are two types of weight loss possible, one is because of attack of HCl and other because of the attack of NaOH. The NaOH attacks the polymer resin materials, while HCl attacks the metal to form ferrous oxide. Weight loss due to the HCl is possible when the edges of panel are open to outside environment. As shown in the Fig. 7, the major weight loss is found because of attack of NaOH, but this weight loss rate is found to be reduced with an increase in the addition of nanocontainer. Compared to NaOH, the weight loss due to acid is very low indicating that the metal is not being exposed directly due to HCl attack and the edges are not sealed, in fact the corrosion occurs only through the edges and hence is very small and the rest of the surface is adequately protected.

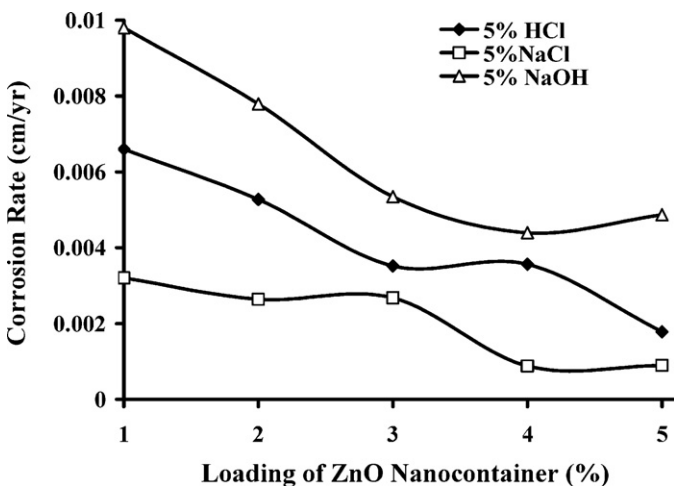


Fig. 7. Effect of loading of nanocontainer on the corrosion rate after loading into the alkyd resin.

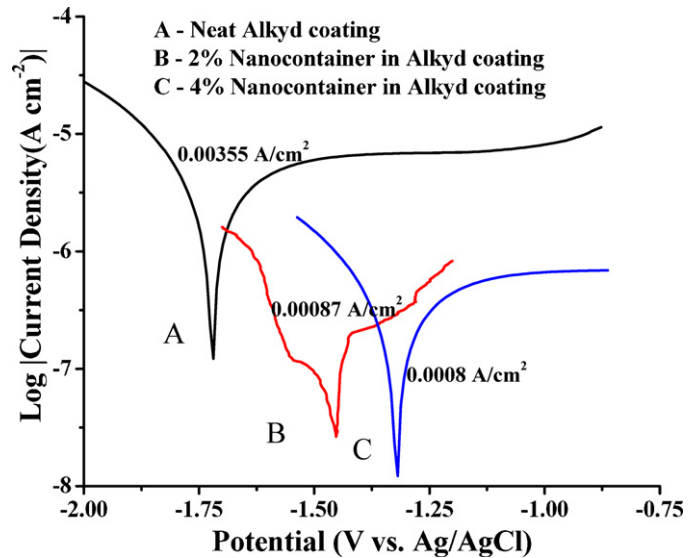


Fig. 8. Tafel plots of mild steel samples coated with different composite material in 5 wt% KCl solution.

Fig. 7 shows the corrosion rate per year at different wt% loading of ZnO nanocontainers in alkyd resin. The synthesized ZnO nanocontainers were incorporated in alkyd resin and were then coated on MS plates for salt solution analysis. MS plates were then dipped in HCl, NaCl and NaOH solutions for a period of 168 h. The weight loss after corrosion was determined by gravimetric analysis. Corrosion rate for 0% loading of ZnO nanocontainer is 0.87 cm/yr, 0.76 cm/yr and 1.024 cm/yr in case of 5% HCl, NaCl and NaOH solution respectively. From Fig. 7, which also show the effect of % loading of ZnO nanocontainer, it can be concluded that the corrosion rate was minimum for NaCl solution and maximum for NaOH solution. The corrosion rate in NaOH solution is the maximum at different % loading of ZnO nanocontainer because the alkyd resin and PAA (outer layer of the nanocontainer) selected are acidic in nature. Due to this the reaction rate between acid and alkali is significant, which leads to maximum corrosion rate of the coating in NaOH solution. With an increase in the percentage loading of ZnO nanocontainers from 2% to 5% as reported in Fig. 7, the corrosion resistance efficiency towards HCl, NaCl and NaOH solution increases and minimum corrosion rate is observed. Hence, it can be concluded that the corrosion resistance reaches a maximum value (minimum corrosion rate) in salt (NaCl) solution.

### 3.3. Comparative study of electrochemical characterization of Nanocontainer containing alkyd coatings and neat alkyd coating

Although the corrosion current density ( $I_{corr}$ ) cannot be measured directly, it can be estimated using a Tafel plot, as shown in Fig. 8, for alkyd resin samples and the samples coated with 4 and 5 wt% composites of nanocontainer dispersed in alkyd resin, in 5 wt% aqueous KCl solutions. For these experiments, uncoated and coated steel strips were used as the working electrodes. In corrosion processes, as with any redox system, cathodic and anodic reactions occur simultaneously. The Tafel plot ( $E$  as a function of  $\log(|I|)$ , where  $I$  represents the total measured current density, i.e.,  $I_c + I_a$ ) can isolate these two processes. It has been found that electrochemical current density decreased from 0.00355 to 0.0008 A/cm<sup>2</sup>, when neat alkyd resin combined with 5% nanocontainers has been used in the coating (tested in KCl electrolyte solution). Additionally,  $E_{corr}$  value show a shift in positive side from -2.0 to 1.0V by the addition of 5 wt% nanocontainer into alkyd coating. Overall results indicate that nanocontainer shows a significant improvement in



### Benzotriazole Inhibits Corrosion of MS Panel by Forming an Inert Layer on the MS Surface by Passivation

Fig. 9. Release mechanism of corrosion inhibitor (benzotriazole) in the polymer.

anticorrosive properties which supports the earlier corrosion rate data obtained by dip test method.

#### 3.4. Release mechanism of the inhibitor in the polymer

Benzotriazole acts as an inhibitor for ferrous metals under acidic conditions [43–45] as well as under neutral conditions [47,48]. Benzotriazole is one of the corrosion inhibitors which protects the metal surface from corrosion by a passivation phenomenon of alkyd coating on the surface by chemisorption. In acidic solutions, the inhibition of iron results from the adsorption of benzotriazole in its molecular or protonated form resulting in the formation of compact passive layer [45,46]. Further, the inhibitive action of organic compounds containing S, N and O is due to the formation of a dative covalent type bond between the metal and the lone pair of electrons in the additive [45,46]. Due to this tendency of bond formation, the scope of inhibition is improved with an increase in the effective electron density of the functional group of the additive [44]. The chemisorption of benzotriazole derivatives on the MS surface can take place on the basis of donor–acceptor interactions between the p-electrons of the inhibitor and the vacant d-orbitals of iron surface atoms [47]. The release mechanism of benzotriazole has been depicted schematically in Fig. 9. The release of benzotriazole takes place in the presence of corrosion medium (pH 3, 5 and 7). As reported earlier, benzotriazole gives better corrosion inhibition in acidic medium and hence the release of benzotriazole has been tested under conditions of pH 3, 5 and 7. The formation of the chemisorption passive layer, consisting of a complex between metal (in this case mild steel) and benzotriazole, takes place on MS surface when benzotriazole gets released from ZnO nanocontainer in the polymer/alkyd coatings. The formed passive layer on MS panel inhibits the attack of corrosion species, which results in the improvement in the anticorrosion performance of ZnO nanocontainer/alkyd coating.

#### 4. Conclusions

The present work has successfully demonstrated the method of formation of nanocontainers using LBL assembly as well as the release mechanism of corrosion inhibitor. LBL assembly has been successfully prepared using ZnO as a core and PANI, polyacrylic acid polyelectrolyte as shell trapping benzotriazole between the layers. Benzotriazole has been encapsulated into the prepared nanocontainer assembly. The prepared nanocontainers are consistent in release of liquid anticorrosion agent over 8 h, though release study

was carried out only in aqueous media at different pH. Zeta potential and particle size relationship shows that the layer by layer assembly is well encapsulated and shows appropriate change in the surface charge which could be responsible for the release mechanism when initiated by the change in pH. Corrosion results from Tafel plot and corrosion rate analysis shows that the 5 wt% loading of nanocontainers is useful and optimum for the sustained release of inhibitor for different applications irrespective of the operating pH.

#### Acknowledgments

Dr. S.H. Sonawane and Prof. A.B. Pandit, Prof R.D. Kulkarni acknowledges the Department of Science and Technology (DST), Government of India, for providing the Funds through Project Grant Reference No: SR/S3/CE/0060/2010. Authors are also thankful to Dr Anand Gole and Dr Sumant Phadtare of Tata Chemicals, Pune for their help in Dynamic Light Scattering and Zeta Potential Analysis.

#### References

- [1] R.W. Revie, Corrosion, Corrosion Control, 4th ed., John Wiley & Sons, New Jersey, 2008.
- [2] P.R. Roberge, Corrosion Engineering, McGraw-Hill, 2008.
- [3] P.A. Schweitzer, Paint and Coatings: Applications and Corrosion Resistance, CRC Press, 2006.
- [4] D. Borisova, H. Mohwald, D.G. Shchukin, Mesoporous silica nanoparticles for active corrosion protection, ACS Nano 5 (2011) 1939–1946.
- [5] E.B. Murphy, F. Wudl, The world of smart healable materials, Prog. Polym. Sci. 35 (2010) 223–251.
- [6] D.Y. Wu, S. Meure, D. Solomon, Self-healing polymeric materials: a review of recent developments, Prog. Polym. Sci. 33 (2008) 479–522.
- [7] J. Tedim, S.K. Poznyak, A. Kuznetsova, D. Raps, T. Hack, M.L. Zheludkevich, M.G.S. Ferreira, Enhancement of active corrosion protection via combination of inhibitor-loaded nanocontainers, Appl. Mater. Inter. 2 (2010) 1528–1535.
- [8] M.L. Zheludkevich, D.G. Shchukin, K.A. Yasakau, H. Möhwald, G.S. Mario, Anticorrosion coatings with self-healing effect based on nanocontainers impregnated with corrosion inhibitor, Chem. Mater. 19 (2007) 402–411.
- [9] Y. Hu, Y. Chen, Q. Chen, L. Zhang, X. Jiang, C. Yang, Synthesis and stimuli-responsive properties of chitosan/poly(acrylic acid) hollow nanospheres, Polymers 46 (2005) 12703–12710.
- [10] M. Evaggelos, K. Ioannis, P. George, K. George, release studies of corrosion inhibitors from cerium titanium oxide nanocontainers, J. Nanopart. Res. 13 (2011) 541–554.
- [11] M.L. Zheludkevich, R. Serra, M.F. Montemor, M.G.S. Ferreira, Oxide nanoparticle reservoirs for storage and prolonged release of corrosion inhibitors, Electrochem. Commun. 7 (2005) 836–840.
- [12] C. Suryanarayana, K.C. Rao, D. Kumar, Preparation and characterization of microcapsules containing linseed oil and its use in self-healing coatings, Prog. Org. Coat. 63 (2008) 72–78.

- [13] T. Nesterova, K. Dam-Johansen, S. Kiil, Synthesis of durable microcapsules for self-healing anticorrosive coatings: a comparison of selected methods, *Prog. Org. Coat.* 70 (2011) 342–352.
- [14] S. Benito, A. Graff, R. Stoescu, P. Broz, C. Saw, H. Heider, S. Marsch, P. Hunziker, W. Meier, Polymer nanocontainers for biomedical applications, *Eur. Cell. Mater.* 6 (2003) 21–22.
- [15] J. Yang, J. Lee, J. Kang, K. Lee, J. Suh, H. Yoon, Y. Huh, S. Haam, Hollow silica nanocontainers as drug delivery vehicles, *Langmuir* 24 (2008) 3417–3421.
- [16] C. George, D. Dorfs, G. Bertoni, A. Falqui, A. Genovese, T. Pellegrino, A. Roig, A. Quarta, R. Comparelli, M.L. Curri, R. Cingolani, L. Manna, A cast-mold approach to iron oxide and Pt/iron oxide nanocontainers and nanoparticles with a reactive concave surface, *J. Am. Chem. Soc.* 133 (2011) 2205–2217.
- [17] A. Kumar, L.D. Stephenson, J.N. Murray, Self-healing coatings for steel, *Prog. Org. Coat.* 55 (2006) 244–253.
- [18] K. Aramaki, Self-healing mechanism of an organosiloxane polymer film containing sodium silicate and cerium (III) nitrate for corrosion of scratched zinc surface in 0.5 M NaCl, *Corros. Sci.* 44 (2002) 1621–1632.
- [19] G. Paliwoda-Porebska, M. Stratmann, M. Rohwerder, K. Potje-Kamloth, Y. Lu, A.Z. Pich, On the development of polypyrrole coatings with self-healing properties for iron corrosion protection, *Corros. Sci.* 47 (2005) 3216–3233.
- [20] D.G. Shchukin, M. Zheludkevich, K. Yasakau, S. Lamaka, M.G.S. Ferreira, H. Mowald, Layer-by-layer assembled nanocontainers for self healing corrosion protection, *Adv. Mater.* 18 (2006) 1672–1678.
- [21] I.A. Kartsonakis, G. Kordas, Synthesis and characterization of cerium molybdate nanocontainers and their inhibitor complexes, *J. Am. Ceram. Soc.* 93 (2009) 65–73.
- [22] D.G. Shchukin, S.V. Lamaka, K.A. Yasakau, M.L. Zheludkevich, M.G.S. Ferreira, H. Mowald, Active anticorrosion coatings with halloysite nanocontainers, *J. Phys. Chem. C* 112 (2008) 958–964.
- [23] D.G. Shchukin, H. Mowald, Surface-engineered nanocontainers for entrapment of corrosion inhibitors, *Adv. Funct. Mater.* 17 (2007) 1451–1458.
- [24] Y.M. Abu, K. Aoki, Corrosion protection by polyaniline-coated latex microspheres, *J. Electroanal. Chem.* 583 (2005) 133–139.
- [25] D.G. Shchukin, M. Zheludkevich, H. Mowald, Feedback active coatings based on incorporated nanocontainers, *J. Mater. Chem.* 16 (2006) 4561–4566.
- [26] M. Tomalino, G. Bianchini, Heat-expandable microspheres for car protection production, *Prog. Org. Coat.* 32 (1997) 17–24.
- [27] D.J. Bell, Y. Sun, L. Zhang, L.X. Dong, B.J. Nelson, D. Grutzmacher, Three-dimensional nanosprings for electromechanical sensors, in: *Proc. of the 13th Int. Conf. on Solid-State Sensors, Actuators and Microsystems*, Seoul, June 5–9, 2005, pp. 15–18.
- [28] M. Yasuda, N. Akao, N. Hara, K. Sugimoto, Self-healing corrosion protection ability of composition-gradient  $\text{Al}_2\text{O}_3/\text{Nb}$  nanocomposite thin films, *J. Electrochem. Soc.* 150 (2003) B481–B487.
- [29] M. Samadzadeh, S.H. Boura, M. Peikari, S.M. Kasirha, A.A. Ashrafi, Review on self-healing coatings based on micro/nanocapsules, *Prog. Org. Coat.* 68 (2010) 159–164.
- [30] S.H. Sonawane, B.M. Teo, A. Brotchie, F. Grieser, M. Ashokkumar, Sonochemical synthesis of ZnO encapsulated functional nanolatex and its anticorrosive performance, *Ind. Eng. Chem. Res.* 49 (2010) 2200–2205.
- [31] B. Chico, J. Simancas, J. Vega, N. Granizo, I. Diaz, D. De la Fuente, M. Morcillo, Anticorrosive behaviour of alkyd paints formulated with ion-exchange pigments, *Prog. Org. Coat.* 61 (2008) 283–290.
- [32] A. Kalendova, D. Vesely, Study of the anticorrosive efficiency of zincite and periclase-based core-shell pigments in organic coatings, *Prog. Org. Coat.* 4 (2009) 5–19.
- [33] E. Jose, S. Pereira, I. Susana, T. Cordoba, M.T. Roberto, Polyaniline acrylic coatings for corrosion inhibition: the role played by counter-ions, *Corros. Sci.* 47 (2005) 811–822.
- [34] B.A. Bhanvase, S.H. Sonawane, New approach for simultaneous enhancement of anticorrosive and mechanical properties of coatings: application of water repellent nano  $\text{CaCO}_3$ -PANI emulsion nanocomposite in alkyd resin, *Chem. Eng. J.* 156 (2010) 177–183.
- [35] S.S. Barkade, J.B. Naik, S.H. Sonawane, Ultrasound assisted miniemulsion synthesis of polyaniline/Ag nanocomposite and its application for ethanol vapor sensing, *Coll. Surf. A: Physicochem. Eng. Aspects* 378 (2011) 94–98.
- [36] B.J. Kim, S.G. Oh, S.S. Im, Investigation on the solubilization locus of aniline-HCl salt in SDS micelles with  $^1\text{H-NMR}$  spectroscopy, *Langmuir* 17 (2001), 565–266.
- [37] L.P. Salgaonkar, R.V. Jayaram, Polyaniline film formation in hexadecyl trimethyl ammonium bromide admicelles on hydrous zirconia surface, *J. Colloid Interface Sci.* 291 (2005) 92–97.
- [38] A.H. Jafari, S.M.A. Hosseini, E. Jamalizadeh, Investigation of smart nanocapsules containing inhibitors for corrosion protection of copper, *Electrochim. Acta* 55 (2010) 9004–9009.
- [39] M.M. Mennucci, E.P. Banczek, P.R.P. Rodrigues, I. Costa, Evaluation of benzotriazole as corrosion inhibitor for carbon steel in simulated pore solution, *Cem. Concr. Compos.* 31 (2009) 418–424.
- [40] K. Yoshino, T. Fukushima, M. Yoneta Structural, Optical and electrical characterization on ZnO film grown by a spray pyrolysis method, *J. Mater. Sci. Mater. Electron.* 16 (2005) 403–408.
- [41] M. Takeuchi, G. Martra, S. Coluccia, M. Anpo, Investigations of the structure of  $\text{H}_2\text{O}$  clusters adsorbed on  $\text{TiO}_2$  surfaces by near-infrared absorption spectroscopy, *J. Phys. Chem. B* 109 (2005) 7387–7391.
- [42] I. Kartsonakis, I. Danilidis, G. Kordas, Encapsulation of the corrosion inhibitor 8-hydroxyquinoline into ceria nanocontainers, *J. Sol-Gel Sci. Technol.* 48 (2008) 24–31.
- [43] P. Matheswaran, A.K. Ramasamy, Influence of benzotriazole on corrosion inhibition of mild steel in citric acid medium, *E-J. Chem* 7 (2010) 1090–1094.
- [44] S.T. Selvi, V. Raman, N. Rajendran, Corrosion inhibition of mild steel by benzotriazole derivatives in acidic medium, *J. Appl. Electrochem.* 33 (2003) 1175–1182.
- [45] A. Popova, M. Christov, Evaluation of impedance measurements on mild steel corrosion in acid media in the presence of heterocyclic compounds, *Corros. Sci.* 48 (2006) 3208–3221.
- [46] P.G. Cao, J.L. Yao, J.W. Zheng, R.A. Gu, Z.Q. Tian, Comparative study of inhibition effects of benzotriazole for metals in neutral solutions as observed with surface enhanced Raman spectroscopy, *Langmuir* 18 (2002) 100–104.
- [47] S. Ramesh, S. Rajeswari, Corrosion inhibition of mild steel in neutral aqueous solution by new triazole derivatives, *Electrochim. Acta* 49 (2004) 811–820.
- [48] T. Murakawa, S. Nagaura, N. Hackerman, Coverage of iron surface by organic compounds and anions in acid solutions, *Corros. Sci.* 7 (1967) 79–89.